ACS Medicinal Chemistry Letters

pubs.acs.org/acsmedchemlett Letter

Spiroindoline-Capped Selective HDAC6 Inhibitors: Design, Synthesis, Structural Analysis, and Biological Evaluation

A. Prasanth Saraswati,[+] Nicola Relitti,[+] Margherita Brindisi,[+] Jeremy D. Osko, Giulia Chemi, Stefano Federico, Alessandro Grillo, Simone Brogi, Niamh H. McCabe, Richard C. Turkington, Ola Ibrahim, Jeffrey O'Sullivan, Stefania Lamponi, Magda Ghanim, Vincent P. Kelly, Daniela Zisterer, Rebecca Amet, Patricia Hannon, Francesca Vanni, Cristina Ulivieri, Daniel Herp, Federica Sarno, Antonella Di Costanzo, Fulvio Saccoccia, Giovina Ruberti, Manfred Jung, Lucia Altucci, Sandra Gemma, Stefania Butini, David W. Christianson, and Giuseppe Campiani*

Cite This: https://dx.doi.org/10.1021/acsmedchemlett.0c00395 Read Online

ACCESS | Metrics & More | Article Recommendations | Supporting Information

ABSTRACT: Histone deacetylase inhibitors (HDACi) have emerged as promising therapeutics for the treatment of neurodegeneration, cancer, and rare disorders. Herein, we report the development of a series of spiroindoline-based HDAC6 isoform-selective inhibitors based on the X-ray crystal studies of the hit **6a**. We identified compound **6j** as the most potent and selective *h*HDAC6 inhibitor of the series. Biological investigation of compounds **6b**, **6h**, and **6j** demonstrated their antiproliferative activity against several cancer cell lines. Western blotting studies indicated that they were able to increase tubulin acetylation, without significant variation in histone acetylation state, and induced PARP cleavage indicating their apoptotic potential at the molecular level. **6j** induced HDAC6-dependent pSTAT3 inhibition.

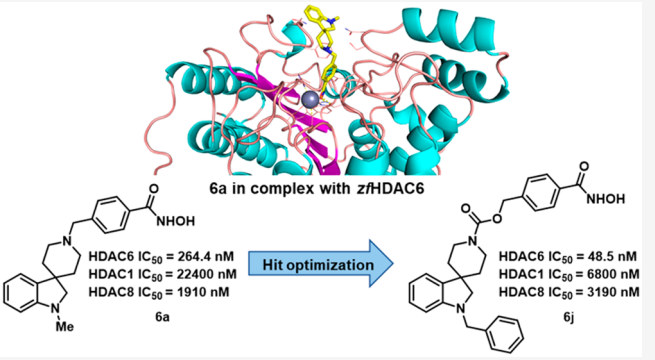

KEYWORDS: *HDAC6, HDAC inhibitors, spiroindoline, cancer therapy, STAT3*

Cancer, diabetes, cardiovascular, neurological, and metabolic disorders have an epigenetic etiology. Histone proteins play a crucial role in organizing the DNA into structures called nucleosomes. Histone acetylation and deacetylation comprise a prime example of post-translational modifications that function in epigenetic regulation. Histone deacetylases (HDAC) remove acetyl groups from lysine residues and thereby regulate key processes such as gene expression.[1] They are clustered in four different classes (I–IV): class I HDAC enzymes consist of isoforms 1, 2, 3, and 8; whereas class II enzymes include the isoforms 4, 5, 6, 7, 9, and 10. Class IV contains only isoform 11, and, similarly to class I and II isoforms, this enzyme is zinc dependent. In contrast, the class III HDACs are NAD^+-dependent enzymes called sirtuins (SIRT isoforms 1–7). A common structural feature of HDAC inhibitors (HDACi) is the presence of a zinc binding group (ZBG), a linker moiety and a cap-group portion. The linker and the cap-group and ZBG can be functionalized to modulate selectivity toward specific HDAC isoforms.[2] Many HDACi have been identified as therapeutic tools for the treatment of various pathologies such as cancer, infectious diseases, neurodegenerative disorders and rare diseases.[3−6] To date, four HDACi pan-inhibitors have been approved by the U.S. Food and Drug Administration (FDA) in cancer therapy: vorinostat (**1**), romidepsin (**2**), panobinostat (**3**), and belinostat (**4**, (Figure 1). Their use may lead to unwanted side effects such as thrombocytopenia, neutropenia, diarrhea, nausea, vomiting, and fatigue as the most commonly detected.[7]

Accordingly, significant research efforts are currently focused on the development of isoform-selective HDACi.[2,6] HDAC6 represents a unique member of the HDAC family due to two main factors: (a) it contains two distinct catalytic domains and is primarily found in the cytoplasm (unlike HDAC1, -2, and -3, which are nuclear localized isoforms and HDAC8, displaying both nuclear and cytoplasmic distribution; interestingly, the cytosolic enzyme HDAC10, which is closely related to HDAC6, is ineffective as a lysine deacetylase);[8] (b) it

Received: July 17, 2020
Accepted: September 29, 2020
Published: September 29, 2020

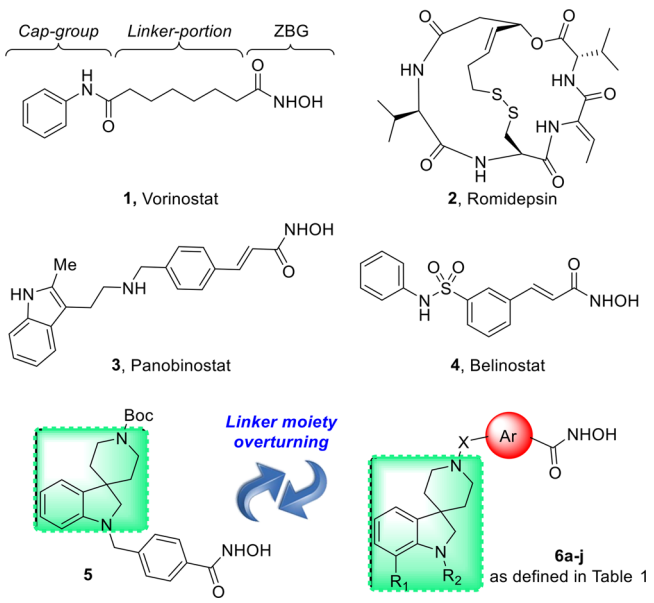

Figure 1. Structures of FDA approved HDAC inhibitors: Vorinostat (**1**), romidepsin (**2**), panobinostat (**3**), and belinostat (**4**), spiroindoline inhibitor **5**, and novel HDAC6i **6a**–**j**.

predominantly acts on non-histone substrates, such as α-tubulin, Hsp90, and cortactin.[2] In spite of a couple of recent reports stating the challenges of using HDAC6i in cancer,[9,10] ample evidence outweighs its utility as anticancer agents.[6,11] In particular, the involvement of HDAC6 in cancer cell migration and metastasis[11] prompted us to develop novel anticancer agents as selective HDAC6 inhibitors. Further, the contribution of non-histone proteins such as α-tubulin and Hsp90 in HDAC6-mediated tumorigenesis makes selective HDAC6 inhibition a unique therapeutic strategy for cancer chemotherapy, with respect to the use of classical pan-HDAC inhibitors.[6]

In an effort to develop potent and selective HDAC6i, our group has recently identified spiroindoline-capped HDACi (**5**, Figure 1) which exhibited significant anticancer potential against several cancer cell lines.[12] In this work, we have investigated the impact of a strategical overturning of the linker and the ZBG moieties from the indoline nitrogen (compound **5**) to the piperidine nitrogen (compounds **6a**–**j**) in order to improve biological properties. The prototype **6a** (Table 1) demonstrated a promising *h*HDAC6 IC_{50} value of 264.4 nM with a selectivity index of 85 over *h*HDAC1 and of 7 over *h*HDAC8. To gain a deeper understanding of the binding mode of **6a** and to proceed to the design of analogues, a 2.09 Å resolution X-ray crystal structure of the complex between **6a** and catalytic domain 2 of HDAC6 from *Danio rerio* (zebrafish)

Table 1. Inhibitory Activity of Compounds 6a–j and Reference Compounds (5 and Tubastatin A) against *h*HDAC1, as IC_{50} (μM), and *h*HDAC6, as IC_{50} (nM)[a]

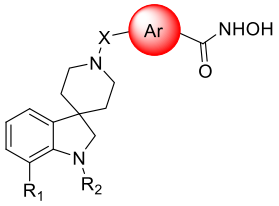

Cpd	R_1	R_2	X	Ar	HDAC1 IC_{50} (μM) or inhibition % @ 1 μM	HDAC6 IC_{50} (nM) or inhibition % @ 1 μM	HDAC1/HDAC6
6a	H	$-CH_3$	$-CH_2-$	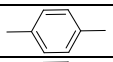	22.4 ± 6	264.4 ± 45	85
6b	H	$-CH_2C_6H_5$	$-CH_2-$	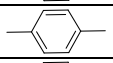	6.5 ± 0.8	561.0 ± 203	12
6c	H	$-COC_6H_5$	$-CH_2-$	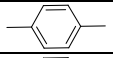	10.1 ± 2.1	155.0 ± 26	65
6d	C_6H_5	$-CH_3$	$-CH_2-$	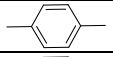	8.5%	50.0%	n.d.
6e	C_6H_5	$-CH_2C_6H_5$	$-CH_2-$	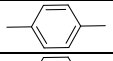	2.9%	29.7%	n.d.
6f	C_6H_5	$-COC_6H_5$	$-CH_2-$	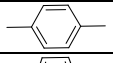	4.7 ± 0.5	465.0 ± 122	10
6g	H	$-CH_3$	$-CH_2-$	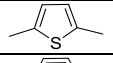	6.6 %	51.3%	n.d.
6h	H	$-CH_2C_6H_5$	$-COCH_2-$	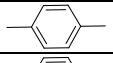	10.2 ± 1	227.0 ± 97	45
6i	H	$-CH_2C_6H_5$	$-CONHCH_2-$	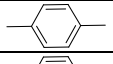	3.6 ± 0.3	110.0 ± 19	33
6j	H	$-CH_2C_6H_5$	$-COOCH_2-$	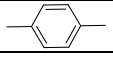	6.8 ± 0.3	48.5 ± 23	140
5[12]	-	-	-	-	4.00 ± 0.78	41.9 ± 7.9	95
tubastatin A	-	-	-	-	1.91 ± 0.42	30.4 ± 2.1	63

[a]Each value is the mean of at least three determinations; compounds were assayed at eight concentrations; results are expressed with SD.

https://dx.doi.org/10.1021/acsmedchemlett.0c00395
ACS Med. Chem. Lett. XXXX, XXX, XXX−XXX

Scheme 1. Synthesis of the Final Compounds 6a−j[a]

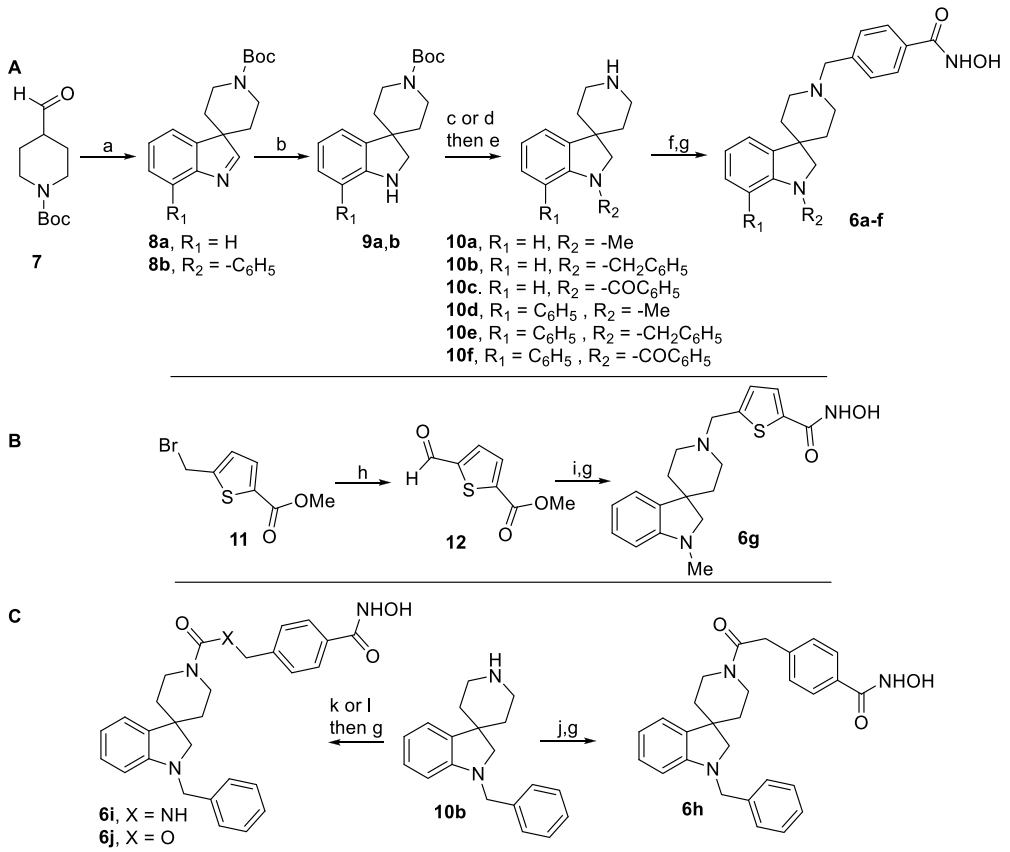

[a]Reagents and conditions: (A) (a) Phenylhydrazine or (1,1-biphenyl)-2-ylhydrazine·HCl, AcOH, 80 °C, 2 h; (b) H_2, Pd/C, MeOH, 25 °C, 3 h; (c) paraformaldehyde or benzaldehyde, $NaBH_3CN$, MeOH, 25 °C, 8 h; (d) benzoyl chloride, TEA, DCM, 25 °C, 1 h; (e) 1 N HCl in MeOH, 25 °C, 15 min; (f) methyl 4-formyl benzoate, $NaBH_3CN$, MeOH, 25 °C, 8 h; (g) NH_2OH (50 wt % in H_2O), 4 M KOH in MeOH, DCM/MeOH, 25 °C, 2 h. (B) (h) NMO, MeCN, 25 °C, 12 h; (i) **10a**, $NaBH_3CN$, MeOH, 25 °C, 8 h. (C) (j) 2-(4-(Methoxycarbonyl)phenyl)acetic acid, EDCI, HOBt, DIPEA, DCM, 0−25 °C, 24 h; (k) methyl 4-(isocyanatomethyl)benzoate, TEA, dry THF, 45 °C, 2 h; (l) methyl 4-(hydroxymethyl)benzoate, CDI, DCM, 0° to 25 °C, 6 h.

was determined. The active site structure of zebrafish HDAC6 (*zf*HDAC6) is essentially identical to that of *h*HDAC6, and *zf*HDAC6 yields crystals of much better quality compared with crystals of *h*HDAC6.[13] Subsequently, molecular modeling approaches were exploited to analyze the binding mode and the structural requirements to design novel "reversed" spiroindolines with an improved HDAC6 inhibitory profile and selectivity index. This was achieved following two main strategies: (i) synthesizing derivatives with bulkier cap-groups and (ii) modulating the outdistancing between the cap-group and the ZBG, through the insertion of amide, urea, and carbamate functionalities in the linker portion. The resulting compounds (**6b−j**) were tested for their ability to inhibit the HDAC1, -6, and -8 isoforms. In addition, the best performing compounds were further evaluated for their effects on cell cycle progression and apoptosis in various cancer cell lines.

For the synthesis of compounds **6a−j**, five key steps were employed to obtain the desired products which include (i) an interrupted Fischer indolization, starting from suitable arylhydrazines and *N*-Boc-piperidine-4-carboxaldehyde providing 3,3-disubstituted indolenines, (ii) reduction of the imine bond of the indolenines to get the respective indolines, (iii) appropriate substitution at the *N*-1 position of the indoline, (iv) insertion at the piperidine nitrogen with suitable linkers, and (v) conversion of the ester into hydroxamic acid (Scheme 1). See the Supporting Information, section 1, for more details.

The 2.09 Å resolution crystal structure of the *zf*HDAC6 CD2-**6a** complex revealed that the inhibitor hydroxamate group coordinates to the catalytic Zn^{2+} with bidentate geometry (Figure 2). The Zn^{2+}-bound hydroxamate C═O group accepts a hydrogen bond from Y745, the Zn^{2+}-bound hydroxamate N−O^- group accepts a hydrogen bond from H573, and the hydroxamate NH group donates a hydrogen bond to H574. This constellation of intermolecular interactions with catalytically relevant residues accounts for the high affinity generally retrieved for the hydroxamate-based inhibitors in the HDAC6 active site.

The *para*-substituted phenyl linker makes favorable offset $\pi-\pi$ interactions in the aromatic crevice defined by F583 and F643. The piperidine ring adopts a chair conformation, and the piperidine nitrogen forms a hydrogen bond with a water molecule that in turn hydrogen bonds with the backbone carbonyl of R798. The spiroindoline group is oriented toward the L2 pocket at the mouth of the active site. There, the indoline nitrogen hydrogen bonds with a water molecule that in turn is linked to N645 and a second water molecule; a third water molecule completes a hydrogen bond network between the indoline nitrogen and Zn^{2+} ligand H614. Although the inhibitor makes no direct enzyme−inhibitor hydrogen bonds

https://dx.doi.org/10.1021/acsmedchemlett.0c00395
ACS Med. Chem. Lett. XXXX, XXX, XXX−XXX

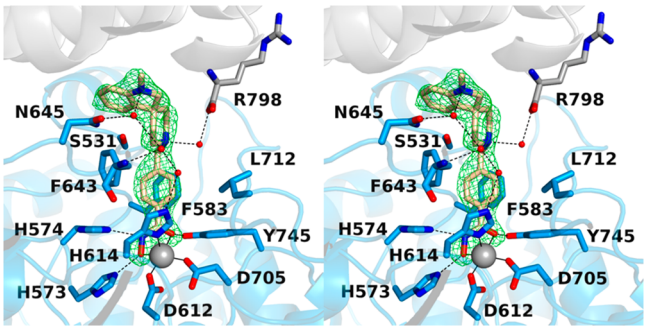

Figure 2. Stereoview of a Polder omit map of the HDAC6-**6a** complex for which the atomic coordinates of **6a** were omitted from the structure factor calculation (PDB 6V7A; contoured at 5.0 σ). Atoms are color-coded as follows: C = light blue (HDAC6 catalytic domain 2), light gray (symmetry mate), or wheat (inhibitor), N = blue, O = red, Zn^{2+} = gray sphere, and solvent = small red spheres. Metal coordination and hydrogen bond interactions are indicated by solid and dashed black lines, respectively.

apart from those made with the hydroxamate moiety, it is interesting that three water molecules comprise a "wet" hydrogen bonded interface in such a high-affinity enzyme–inhibitor pair.

It is relatively rare to see inhibitor capping groups bind in the L2 pocket, since most tend to bind in the L1 pocket on the opposite side of the active site.[14−18] It appears that the chair conformation of the piperidine ring combined with the molecular structure of the novel spiro-fused indoline moiety yields a structure and a conformation that is ideal for binding within the L2 pocket.

A computational investigation (Figure S1) highlighted that **6a** accommodates in a similar fashion in both *zf*HDAC6 and *h*HDAC6 enzymes, with only slight changes. Three main differences could be observed, involving the residues D567, T678, and M682 in *h*HDAC6 which are replaced by N530, A641, and N645 in *zf*HDAC6. The presence of M682 in *h*HDAC6 contributed to a slightly different orientation of the cap-group that is more solvent exposed with respect to the crystal structure and the docked pose within *zf*HDAC6. This study confirms that *zf*HDAC6 could represent a valuable structural model for translating the results of potential inhibitors to *h*HDAC6.

The *in vitro* inhibitory profile of the newly developed compounds **6a−j** (Table 1) was evaluated against *h*HDAC1 and -6. SAR studies were performed by taking into consideration the data obtained from *in vitro*, X-ray, and computational studies. To get a better understanding of the behavior of the compounds in the binding sites of *h*HDAC1 and -6, we performed docking studies based on a previously reported protocol (Figures S2−S9).[3,12] It was observed that the hindrance imposed by a bulkier cap-group allowed the compound to be better accommodated into the HDAC6 enzyme with respect to the HDAC1 isoform.

Based on these studies, limited contacts were established by **6a** within the HDAC1 binding site (Figure 3A) compared to those established within HDAC6 binding site (Figure 3B). **6a** was able to coordinate Zn^{2+} in HDAC1 by its hydroxamic moiety through polar contacts with the backbone of G149 and the side chain of Y303. In addition, we observed only a $\pi-\pi$ stacking with H141 and some hydrophobic interactions with Y204, F205, and L271. On the contrary, the docking output of **6a** into HDAC6 showed an increased number of contacts. The hydroxamic acid moiety coordinated with Zn^{2+} and established supplementary H-bonds with the side chain of Y782 and H610 and with the backbone of G619. The benzyl linker was able to

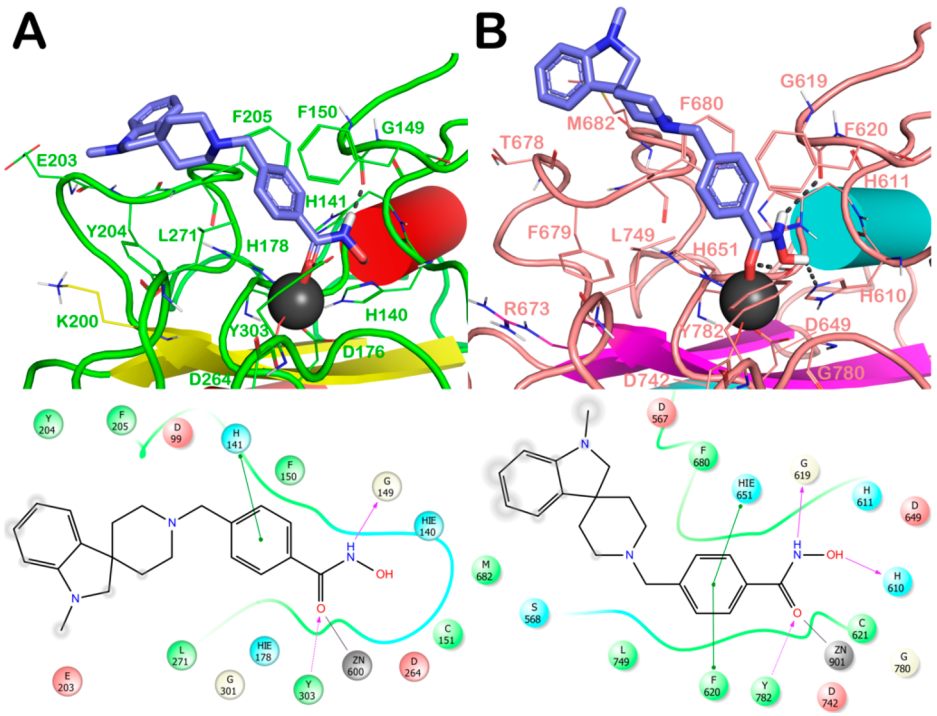

Figure 3. Docked poses of **6a** into HDAC1 (A) and HDAC6 (B). Compound **6a** is represented by purple sticks, the residues in the active sites are represented by lines, and the protein is represented as a cartoon. Zn^{2+} is represented by a gray sphere. H-bonds are shown as black dotted lines, and the red solid lines represent the metal coordination bonds.

https://dx.doi.org/10.1021/acsmedchemlett.0c00395
ACS Med. Chem. Lett. XXXX, XXX, XXX−XXX

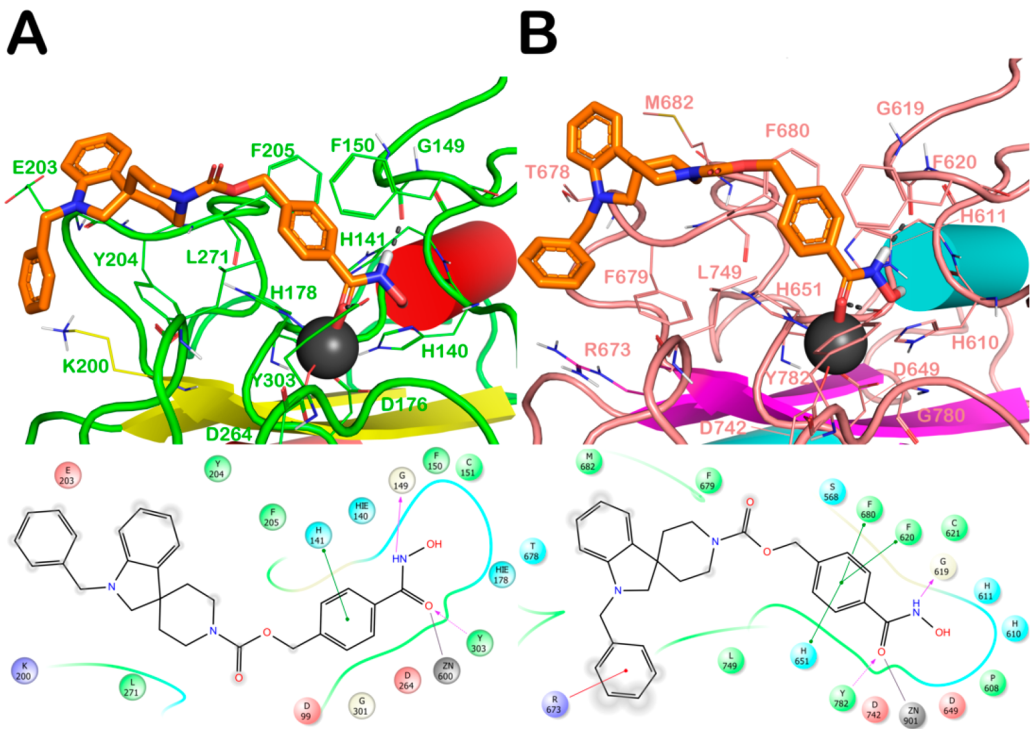

Figure 4. Docked poses of **6j** into HDAC1 (A) and HDAC6 (B). Compound **6j** is represented by orange sticks, the residues in the active sites are represented by lines and the protein is represented as cartoon. Zn^{2+} is represented by a gray sphere. H-bonds are shown as black dotted lines, and the red solid lines represent the metal coordination bonds.

establish a double $\pi-\pi$ stacking with F620 and H651. We also noted relevant hydrophobic interactions with F679, F680, M682, and L749. This pattern of interaction perfectly supported the selectivity of **6a** toward HDAC6 over HDAC1 (IC_{50} HDAC1 = 22.4 μM; IC_{50} HDAC6 = 264.4 nM).

The docking studies of analogues **6b−g** are reported in the Supporting Information, and poses are shown in Figures S1−S8.

In order to investigate the role of the linker portion, compounds **6h−j** were synthesized. **6h**, in addition to the contacts found for **6a**, was able to produce a $\pi-\pi$ stacking with F205 of HDAC1 through the benzyl functionality. In HDAC6, compound **6h** showed the same interactions of **6a** and the crucial $\pi-\pi$ stacking with F680 (IC_{50} HDAC1 = 10.2 μM; IC_{50} HDAC6 = 227 nM). Compound **6i** demonstrated that the urea functionality determines an improvement in inhibitory potency against both isoforms. Therefore, **6i** established two further interactions beside those described for **6h**, namely, (i) a H-bond with the side chain of H178 and (ii) a cation$-\pi$ stacking with K200. With respect to the HDAC6 enzyme, **6i** interacts with the same residues described for **6h**, displaying an additional H-bond between the side chain of S568 and the urea NH (IC_{50} HDAC1 = 3.6 μM; IC_{50} HDAC6 = 110 nM).

The carbamic functionality of **6j** determined an improvement in potency and selectivity toward HDAC6 over HDAC1 (Figure 4). The hydroxamic acid moiety, in addition to the metal coordination bond with the Zn^{2+}, established a series of H-bonds with the side chain of Y782 and with the backbone of G619 of HDAC6. Moreover, its benzyl linker established a triple $\pi-\pi$ stacking with F620, F680, and H651. Also, relevant hydrophobic interactions with T678, F679, M682, and L749 were observed. Notably, the phenyl group of the indole established a cation$-\pi$ stacking with R673 (IC_{50} *h*HDAC1 = 6.8 μM; IC_{50} *h*HDAC6 = 48 nM; IC_{50} *h*HDAC8 = 3.9 μM).

6a, **6i**, and **6j** were tested on the *h*HDAC8 isoform (Table 2), and their selective profile was confirmed toward the HDAC6 enzyme.

Table 2. Inhibitory Activity of 6a, 6i, and 6j, as IC_{50} (μM), against *h*HDAC8[a]

compd	**6a**	**6i**	**6j**	TubA[12]
IC_{50} (μM)	1.91 ± 0.33	2.48 ± 0.67	3.19 ± 1.51	0.695

[a]Each value is the mean of at least three determinations; compounds were assayed at eight concentrations; results are expressed with SD.

We also investigated the potential affinity toward HDAC10 of the new compounds. We used the crystallized structure of the mentioned enzyme from *Danio rerio* due to the high identity with the human enzyme, especially in the binding site (sequence identity >44%; sequence similarity >65%) (PDB ID 6WBQ).[19] The output of this calculation is presented in Figures S10 and S11. In general, we observed that our molecules are poor binders of *zf*HDAC10 enzyme, indicating that HDAC10 is not a preferred target for this series of derivatives, confirming HDAC6 as the main target (see Supporting Information section 4.4).

In a range of malignancies, HDAC6 has been found to be overexpressed and shown to correlate with increased tumor aggressiveness including oral squamous cell carcinoma[20] and esophageal squamous cell carcinoma.[21] Therefore, the new molecules were tested against leukemic, multiple myeloma, oral, and esophageal cancer cells to evaluate their antiproliferative activity and mechanism of action. Cell cycle distribution and propidium iodide (PI) analysis studies were performed on U937 and NB4 cell lines, with selected compounds **6b**, **6h**, and **6j**. Specifically, in U937 cells, **6b** exhibited cell death and a significant S phase reduction at a concentration of 10 μM

https://dx.doi.org/10.1021/acsmedchemlett.0c00395
ACS Med. Chem. Lett. XXXX, XXX, XXX−XXX

(Figure S15A). **6j** (10 μM) only after 48 h of treatment induces an increase of the pre-G1 phase, without significant cell cycle variation (Figure S15B). Interestingly, in the NB4 cell line, both **6b** and **6h** displayed a similar phenotypic effect in terms of cell death at the two time intervals 24 and 48 h (Figure S16A, B), whereas **6j** show this only at 48 h of treatment (Figure S16C). Western blot analyses on NB4 total cell extracts using compounds **6b**, **6h**, and **6j** were also performed. Induction of acetylated tubulin was observed without a significant variation in histone acetylation state (Figure S16D−F), which was detected only after treatment with **6h** and **6j** at higher concentration, thus confirming selective HDAC6 inhibition. Moreover, cleavage of PARP at 24 h by all molecules indicated apoptosis at a molecular level at both 24 and 48 h at 10 μM concentration (Figure S16D−F). **6a**, **6i**, and **6j** were preliminarily screened against the multiple myeloma (U266) cell line. All three compounds reduced the viability of U266 cells with **6j** exhibiting the greatest potency (IC_{50} = 20.25 μM, Figure S17 and Table 5 SI). Flow cytometric analysis of these compounds in annexin V/PI stained U266 cells showed an induction of apoptotic cell death, with compound **6j** exhibiting the highest potency (Figure S18).

STAT3 represents an important signal transducer and transcription factor displaying a key role in the tumorigenic process. This has been confirmed by the fact that 70% of cancers express activated STAT3.[22,23] Recent reports highlighting the important crosstalk between HDAC6 and STAT3 demonstrated that HDAC6 inhibition leads to a decrease of pSTAT3 and reduce the expression of STAT3-targeted genes.[24] The enhanced survival of leukemic cells in chronic lymphocytic leukemia and in multiple myeloma has been associated with the constitutive activation of the JAK/STAT3 signaling pathway.[22,23] Therefore, we proceeded to test STAT3 inhibition using the HDAC6 inhibitors **6a** and **6j** at 5 and 10 μM concentrations in the human chronic lymphocytic leukemia cell line (MEC1)[23] and at 25 μM against multiple myeloma cells (U266).[22] Both compounds showed a marked decrease in the levels of pSTAT3 in both cell lines. Specifically, **6j** demonstrated the most potent activity with a dose-dependent effect (Figure 5).

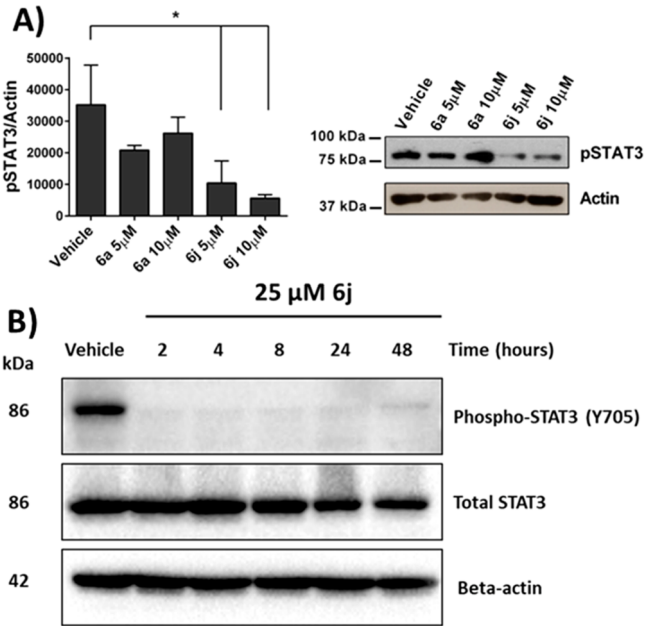

Figure 5. (A) Immunoblot analysis of pSTAT3 in MEC-1 cells treated with **6a** or **6j** (5 or 10 μM) for 30 h. Actin was used as a loading control. The histogram shows the quantification by densiometric analysis of the levels of pSTAT3 relative to actin (n = 2). Data are presented as mean value ± SD. One way ANOVA; *p < 0.05. (B) Immunoblot analysis of pSTAT3 in U266 cells treated with **6j** (25 μM) for 4, 8, 16, 24, and 48 h. Actin was used as a loading control. The blot is representative of three independent experiments with similar results.

Our compounds were also screened against KYSE520 (esophageal squamous cell carcinoma), OE33 (esophageal adenocarcinoma), Ca9-22 (gingival squamous cell carcinoma), and TR-146 (buccal mucosa squamous cell carcinoma) cell lines. **6b** demonstrated the highest activity against KYSE520 (IC_{50} = 12.76 μM), OE33 (IC_{50} = 5.56 μM), Ca9-22 (IC_{50} = 19.00 μM), and TR-146 (IC_{50} = 18.00 μM, Supporting Information, section 6) cell lines. Flow cytometric analysis established that **6b** was able to trigger apoptosis after 48 h of treatment in the KYSE520 cell line.

Furthermore, cytotoxicity assays were performed on compounds **6a** and **6b** to establish the effect on mouse fibroblasts NIH3T3. Compound **6b** showed a TC_{50} of 40 μM being slightly less toxic than **6a** and **6j** (TC_{50} of 24−27 μM, Tables 6 and 7 in the Supporting Information). Potential mutagenicity caused by the use of hydroxamic-based compounds remains a major concern affecting their druglike profile.[25] To asses this property, the Ames test was carried out. Compounds **6a** and **6b** showed no mutagenic effect on the TA98 strain (with or without S9 activation), while low mutagenicity on the TA100 strain (above 8 μM for compound **6b** or above 24− 40 μM for compounds **6a** and **6j** as shown in the Supporting Information, section 9.1) was detected. This effect has been reported also for FDA approved HDACi (**1**-**4**), and it is mostly ascribable to the Lossen rearrangement of the hydroxamate group, generating reactive isocyanates, which can trigger mutagenicity by damaging the DNA.[26]

In summary we have developed a new series of HDAC6 selective inhibitors rationally designed based on the crystallographic study of compound **6a** in complex with *Zf*HDAC6. Compound **6j** resulted the best inhibitor of this series (IC_{50} = 48.5 nM, selectivity index of 140 over HDAC1 and 66 over HDAC8). Notably, the selectivity of these compounds toward HDAC6 over HDAC8 is in general higher respect to the previously published spiroindoline-based HDAC6 inhibitors. Cell-based studies on compounds **6a**, **6b**, **6h**, and **6j** uncovered their antiproliferative activity against several cancer cell lines. We believe that the low of activity in cell-based assays for compound **6j** could be ascribable to the weak stability of the carbamate moiety during the study, which determines the decomposition of the molecule. Oral and esophageal cancers are usually refractory to most of the current therapeutic treatments; notably, our HDAC6 selective inhibitors displayed promising effect in various oral and esophageal cancer cell lines (KYSE520, OE33, Ca9-22, TR-146, and U266B, Table 3). For compounds **6h**, **6b**, and **6j**, PARP cleavage was quantified in NB4 cell extracts, thus indicating its proapoptotic potential at the molecular level. The increased levels of tubulin acetylation without a significant variation in histone acetylation status confirmed the selectivity of **6h**, **6b**, and **6j** for the HDAC6 isoform. Moreover, **6j** was able to inhibit the phosphorylation of STAT3 in MEC1 and U266 cell lines. The studies herein discussed may pave the way for the structure-based design of

https://dx.doi.org/10.1021/acsmedchemlett.0c00395
ACS Med. Chem. Lett. XXXX, XXX, XXX−XXX

Table 3. Antiproliferative Activities of Compounds 6a−b and 6h−j against KYSE520, OE33, Ca9-22, TR-146, and U266B Cell Lines after 48−72 h of Drug Treatment

	IC_{50} (μM)[a]				
compd	KYSE520	OE33	Ca9-22	TR-146	U266B
6a	197	17.73	>1000	>1000	
6b	12.76	5.56	19	18	
6c			>1000	>1000	
6h	33.81	13.82	>1000	54	
6i			55	>1000	59.38
6j		37.83	>1000	133	20.25

[a]Each value is the mean of at least three determinations.

novel HDAC6i as anticancer agents endowed with promising potentialities in the treatment of esophageal and oral cancers.

■ ASSOCIATED CONTENT

Supporting Information

The Supporting Information is available free of charge at https://pubs.acs.org/doi/10.1021/acsmedchemlett.0c00395.

Supplementary figures, details of the synthetic chemistry, *in silico* studies, and biological assays, plot of ^{1}H and ^{13}C NMR spectra (PDF)

■ AUTHOR INFORMATION

Corresponding Author

Giuseppe Campiani − *Department of Biotechnology, Chemistry and Pharmacy, DoE Department of Excellence 2018-2022, University of Siena, I-53100 Siena, Italy;* orcid.org/0000-0001-5295-9529; Phone: (+39) 0577 232239; Email: campiani@unisi.it

Authors

A. Prasanth Saraswati − *Department of Biotechnology, Chemistry and Pharmacy, DoE Department of Excellence 2018-2022, University of Siena, I-53100 Siena, Italy*

Nicola Relitti − *Department of Biotechnology, Chemistry and Pharmacy, DoE Department of Excellence 2018-2022, University of Siena, I-53100 Siena, Italy;* orcid.org/0000-0001-9783-8966

Margherita Brindisi − *Department of Biotechnology, Chemistry and Pharmacy, DoE Department of Excellence 2018-2022, University of Siena, I-53100 Siena, Italy;* orcid.org/0000-0001-9119-3773

Jeremy D. Osko − *Roy and Diana Vagelos Laboratories, Department of Chemistry, University of Pennsylvania, Philadelphia, Pennsylvania 19104-6323, United States*

Giulia Chemi − *Department of Biotechnology, Chemistry and Pharmacy, DoE Department of Excellence 2018-2022, University of Siena, I-53100 Siena, Italy;* orcid.org/0000-0002-3868-6752

Stefano Federico − *Department of Biotechnology, Chemistry and Pharmacy, DoE Department of Excellence 2018-2022, University of Siena, I-53100 Siena, Italy*

Alessandro Grillo − *Department of Biotechnology, Chemistry and Pharmacy, DoE Department of Excellence 2018-2022, University of Siena, I-53100 Siena, Italy*

Simone Brogi − *Department of Pharmacy, University of Pisa, 56126 Pisa, Italy;* orcid.org/0000-0001-9375-6242

Niamh H. McCabe − *Centre for Cancer Research and Cell Biology, Queens University Belfast, Belfast, U.K.*

Richard C. Turkington − *Centre for Cancer Research and Cell Biology, Queens University Belfast, Belfast, U.K.*

Ola Ibrahim − *School of Dental Science, Trinity College Dublin, Dublin 2, Ireland*

Jeffrey O'Sullivan − *School of Dental Science, Trinity College Dublin, Dublin 2, Ireland*

Stefania Lamponi − *Department of Biotechnology, Chemistry and Pharmacy, DoE Department of Excellence 2018-2022, University of Siena, I-53100 Siena, Italy*

Magda Ghanim − *School of Biochemistry and Immunology, Trinity Biomedical Science Institute, Trinity College, Dublin 2, Ireland*

Vincent P. Kelly − *School of Biochemistry and Immunology, Trinity Biomedical Science Institute, Trinity College, Dublin 2, Ireland*

Daniela Zisterer − *School of Biochemistry and Immunology, Trinity Biomedical Science Institute, Trinity College, Dublin 2, Ireland*

Rebecca Amet − *School of Biochemistry and Immunology, Trinity Biomedical Science Institute, Trinity College, Dublin 2, Ireland*

Patricia Hannon − *School of Biochemistry and Immunology, Trinity Biomedical Science Institute, Trinity College, Dublin 2, Ireland*

Francesca Vanni − *Department of Life Sciences, University of Siena, I-53100 Siena, Italy*

Cristina Ulivieri − *Department of Life Sciences, University of Siena, I-53100 Siena, Italy*

Daniel Herp − *Institute of Pharmaceutical Sciences, Albert-Ludwigs-Universität Freiburg, 79104 Freiburg, Germany*

Federica Sarno − *Department of Precision Medicine, University of Campania "Luigi Vanvitelli", 80138 Naples, Italy*

Antonella Di Costanzo − *Department of Precision Medicine, University of Campania "Luigi Vanvitelli", 80138 Naples, Italy*

Fulvio Saccoccia − *Institute of Biochemistry and Cell Biology (IBBC), National Research Council (CNR), 00015 Rome, Italy*

Giovina Ruberti − *Institute of Biochemistry and Cell Biology (IBBC), National Research Council (CNR), 00015 Rome, Italy;* orcid.org/0000-0003-2367-9709

Manfred Jung − *Institute of Pharmaceutical Sciences, Albert-Ludwigs-Universität Freiburg, 79104 Freiburg, Germany;* orcid.org/0000-0002-6361-7716

Lucia Altucci − *Department of Precision Medicine, University of Campania "Luigi Vanvitelli", 80138 Naples, Italy*

Sandra Gemma − *Department of Biotechnology, Chemistry and Pharmacy, DoE Department of Excellence 2018-2022, University of Siena, I-53100 Siena, Italy;* orcid.org/0000-0002-8313-2417

Stefania Butini − *Department of Biotechnology, Chemistry and Pharmacy, DoE Department of Excellence 2018-2022, University of Siena, I-53100 Siena, Italy;* orcid.org/0000-0002-8471-0880

David W. Christianson − *Roy and Diana Vagelos Laboratories, Department of Chemistry, University of Pennsylvania, Philadelphia, Pennsylvania 19104-6323, United States;* orcid.org/0000-0002-0194-5212

Complete contact information is available at: https://pubs.acs.org/10.1021/acsmedchemlett.0c00395

Author Contributions

[+]A.P.S., N.R., and M.B. contributed equally to this work.

https://dx.doi.org/10.1021/acsmedchemlett.0c00395
ACS Med. Chem. Lett. XXXX, XXX, XXX−XXX

Notes

The authors declare no competing financial interest.

The atomic coordinates and crystallographic structure factors of the HDAC6 complex with inhibitor **6a** has been deposited in the Protein Data Bank (www.rcsb.org) with accession code 6V7A. Authors will release the atomic coordinates and experimental data upon article publication.

■ ACKNOWLEDGMENTS

Support from the European Union's Horizon 2020 (EU) Research and Innovation Programme under the Marie Sklodowska-Curie grant agreement No. 721906-TRACT is acknowledged. Cost Action EPICHEMBIO CM1406 (G.C, M.B.). The synchrotron beamline staff at the Advanced Photon Source (APS) for assistance, especially David Neau are also gratefully acknowledged. We thank the Northeastern Collaborative Access Team (NE-CAT) funded by the National Institute of General Medical Sciences (NIGMS) from the NIH (P30 GM124165), and US National Institutes of Health grant GM49758. The Pilatus 6M detector on beamline 24-ID-C is funded by a NIH-ORIP HEI grant (S10 RR029205). This research used resources of the Advanced Photon Source (APS), a U.S. Department of Energy (DOE) Office of Science User Facility operated for the DOE Office of Science by Argonne National Laboratory under Contract No. DE-AC02-06CH11357. N.R. Tuscany strategic project POR-FSE 2014-2020, 'Medicina di Precisione e Malattie Rare'(MePreMaRe), (ACE-ESCC). G.R. acknowledges the CNR-CNCCS "Rare, Neglected and Poverty Related Diseases - Schistodiscovery Project" (DSB.AD011.001.003). L.A. acknowledges MIUR20152TE5PK; VALERE: Vanvitelli per la Ricerca; Campania Regional Government Technology Platform Lotta alle Patologie Oncologiche: iCURE and Campania Regional Government FASE2: IDEAL. MIUR, Proof of Concept POC01_00043.

■ ABBREVIATIONS

HDAC, histone deacetylase; HDACi, HDAC inhibitors; ZBG, zing binding group; Hsp90, heat shock protein 90; SAR, structure−activity relationship; KYSE520, esophageal squamous cell carcinoma; OE33, esophageal adenocarcinoma; Ca9-22, gingival squamous cell carcinoma; TR-146, buccal mucosa squamous cell carcinoma; PI, propidium iodide; U937, monocytic leukemia; NB4, acute promyelocytic leukemia; PARP, poly(ADP-ribose) polymerase; STAT3, signal transducer and activator of transcription 3; JAK, Janus kinase; MEC1, human chronic lymphocytic leukemia; U266, multiple myeloma cells; NIH3T3, mouse fibroblast

■ REFERENCES

(1) Hassig, C. A.; Schreiber, S. L. Nuclear Histone Acetylases and Deacetylases and Transcriptional Regulation: HATs off to HDACs. *Curr. Opin. Chem. Biol.* **1997**, *1* (3), 300−308.

(2) Brindisi, M.; Saraswati, A. P.; Brogi, S.; Gemma, S.; Butini, S.; Campiani, G. Old but Gold: Tracking the New Guise of Histone Deacetylase 6 (HDAC6) Enzyme as a Biomarker and Therapeutic Target in Rare Diseases. *J. Med. Chem.* **2020**, *63* (1), 23−39.

(3) Brindisi, M.; Cavella, C.; Brogi, S.; Nebbioso, A.; Senger, J.; Maramai, S.; Ciotta, A.; Iside, C.; Butini, S.; Lamponi, S.; Novellino, E.; Altucci, L.; Jung, M.; Campiani, G.; Gemma, S. Phenylpyrrole-Based HDAC Inhibitors: Synthesis, Molecular Modeling and Biological Studies. *Future Med. Chem.* **2016**, *8* (13), 1573−1587.

(4) Saccoccia, F.; Brindisi, M.; Gimmelli, R.; Relitti, N.; Guidi, A.; Prasanth, A.; Cavella, C.; Brogi, S.; Chemi, G.; Papoff, G.; Herp, D.; Jung, M.; Campiani, G.; Gemma, S.; Ruberti, G. Screening and Phenotypical Characterization of Schistosoma Mansoni Histone Deacetylase 8 (SmHDAC8) Inhibitors as Multi-Stage Antischistosomal Agents Histone Deacetylase 8 (Sm HDAC8) Inhibitors as Multi-Stage Anti- a Institute b Department c Department. *ACS Infect. Dis.* **2020**, *6* (1), 100−113.

(5) Landucci, E.; Brindisi, M.; Bianciardi, L.; Catania, L. M.; Daga, S.; Croci, S.; Frullanti, E.; Fallerini, C.; Butini, S.; Brogi, S.; Furini, S.; Melani, R.; Molinaro, A.; Lorenzetti, F. C.; Imperatore, V.; Amabile, S.; Mariani, J.; Mari, F.; Ariani, F.; Pizzorusso, T.; Pinto, A. M.; Vaccarino, F. M.; Renieri, A.; Campiani, G.; Meloni, I. IPSC-Derived Neurons Profiling Reveals GABAergic Circuit Disruption and Acetylated α-Tubulin Defect Which Improves after IHDAC6 Treatment in Rett Syndrome. *Exp. Cell Res.* **2018**, *368* (2), 225−235.

(6) Shen, S.; Kozikowski, A. P. A Patent Review of Histone Deacetylase 6 Inhibitors in Neurodegenerative Diseases (2014−2019). *Expert Opin. Ther. Pat.* **2020**, *30* (2), 121−136.

(7) Gryder, B. E.; Sodji, Q. H.; Oyelere, A. K. Targeted Cancer Therapy: Giving Histone Deacetylase Inhibitors All They Need to Succeed. *Future Med. Chem.* **2012**, *4* (4), 505−524.

(8) Hai, Y.; Shinsky, S. A.; Porter, N. J.; Christianson, D. W. Histone Deacetylase 10 Structure and Molecular Function as a Polyamine Deacetylase. *Nat. Commun.* **2017**, *8* (1), 15368.

(9) Lin, A.; Giuliano, C. J.; Palladino, A.; John, K. M.; Abramowicz, C.; Yuan, M. L.; Sausville, E. L.; Lukow, D. A.; Liu, L.; Chait, A. R.; Galluzzo, Z. C.; Tucker, C.; Sheltzer, J. M. Off-Target Toxicity Is a Common Mechanism of Action of Cancer Drugs Undergoing Clinical Trials. *Sci. Transl. Med.* **2019**, *11* (509), eaaw8412.

(10) Depetter, Y.; Geurs, S.; De Vreese, R.; Goethals, S.; Vandoorn, E.; Laevens, A.; Steenbrugge, J.; Meyer, E.; de Tullio, P.; Bracke, M.; D'hooghe, M.; De Wever, O. Selective Pharmacological Inhibitors of HDAC6 Reveal Biochemical Activity but Functional Tolerance in Cancer Models. *Int. J. Cancer* **2019**, *145* (3), 735−747.

(11) Aldana-Masangkay, G. I.; Sakamoto, K. M. The Role of HDAC6 in Cancer. *J. Biomed. Biotechnol.* **2011**, *2011*, 1.

(12) Brindisi, M.; Senger, J.; Cavella, C.; Grillo, A.; Chemi, G.; Gemma, S.; Cucinella, D. M.; Lamponi, S.; Sarno, F.; Iside, C.; Nebbioso, A.; Novellino, E.; Shaik, T. B.; Romier, C.; Herp, D.; Jung, M.; Butini, S.; Campiani, G.; Altucci, L.; Brogi, S. Novel Spiroindoline HDAC Inhibitors: Synthesis, Molecular Modelling and Biological Studies. *Eur. J. Med. Chem.* **2018**, *157*, 127−138.

(13) Hai, Y.; Christianson, D. W. Histone Deacetylase 6 Structure and Molecular Basis of Catalysis and Inhibition. *Nat. Chem. Biol.* **2016**, *12* (9), 741−747.

(14) Mackwitz, M. K. W.; Hamacher, A.; Osko, J. D.; Held, J.; Schöler, A.; Christianson, D. W.; Kassack, M. U.; Hansen, F. K. Multicomponent Synthesis and Binding Mode of Imidazo[1,2-a]Pyridine-Capped Selective HDAC6 Inhibitors. *Org. Lett.* **2018**, *20* (11), 3255−3258.

(15) Hai, Y.; Christianson, D. W. Histone Deacetylase 6 Structure and Molecular Basis of Catalysis and Inhibition. *Nat. Chem. Biol.* **2016**, *12* (9), 741−747.

(16) Osko, J. D.; Porter, N. J.; Narayana Reddy, P. A.; Xiao, Y.-C.; Rokka, J.; Jung, M.; Hooker, J. M.; Salvino, J. M.; Christianson, D. W. Exploring Structural Determinants of Inhibitor Affinity and Selectivity in Complexes with Histone Deacetylase 6. *J. Med. Chem.* **2020**, *63* (1), 295−308.

(17) Porter, N. J.; Osko, J. D.; Diedrich, D.; Kurz, T.; Hooker, J. M.; Hansen, F. K.; Christianson, D. W. Histone Deacetylase 6-Selective Inhibitors and the Influence of Capping Groups on Hydroxamate-Zinc Denticity. *J. Med. Chem.* **2018**, *61* (17), 8054−8060.

(18) Bhatia, S.; Krieger, V.; Groll, M.; Osko, J. D.; Reßing, N.; Ahlert, H.; Borkhardt, A.; Kurz, T.; Christianson, D. W.; Hauer, J.; Hansen, F. K. Discovery of the First-in-Class Dual Histone Deacetylase−Proteasome Inhibitor. *J. Med. Chem.* **2018**, *61* (22), 10299−10309.

(19) Herbst-Gervasoni, C. J.; Steimbach, R. R.; Morgen, M.; Miller, A. K.; Christianson, D. W. Structural Basis for the Selective Inhibition

https://dx.doi.org/10.1021/acsmedchemlett.0c00395
ACS Med. Chem. Lett. XXXX, XXX, XXX−XXX

of HDAC10, the Cytosolic Polyamine Deacetylase. *ACS Chem. Biol.* **2020**, *15*, 2154.
(20) Sakuma, T.; Uzawa, K.; Onda, T.; Shiiba, M.; Yokoe, H.; Shibahara, T.; Tanzawa, H. Aberrant Expression of Histone Deacetylase 6 in Oral Squamous Cell Carcinoma. *Int. J. Oncol.* **2006**, *29* (1), 117−124.
(21) Cao, J.; Lv, W.; Wang, L.; Xu, J.; Yuan, P.; Huang, S.; He, Z.; Hu, J. Ricolinostat (ACY-1215) Suppresses Proliferation and Promotes Apoptosis in Esophageal Squamous Cell Carcinoma via MiR-30d/PI3K/AKT/MTOR and ERK Pathways. *Cell Death Dis.* **2018**, *9* (8), 817.
(22) Catlett-Falcone, R.; Landowski, T. H.; Oshiro, M. M.; Turkson, J.; Levitzki, A.; Savino, R.; Ciliberto, G.; Moscinski, L.; Fernández-Luna, J. L.; Nuñez, G.; Dalton, W. S.; Jove, R. Constitutive Activation of Stat3 Signaling Confers Resistance to Apoptosis in Human U266 Myeloma Cells. *Immunity* **1999**, *10* (1), 105−115.
(23) Stacchini, A.; Aragno, M.; Vallario, A.; Alfarano, A.; Circosta, P.; Gottardi, D.; Faldella, A.; Rege-Cambrin, G.; Thunberg, U.; Nilsson, K.; Caligaris-Cappio, F. MEC1 and MEC2: Two New Cell Lines Derived from B-Chronic Lymphocytic Leukaemia in Prolymphocytoid Transformation. *Leuk. Res.* **1999**, *23* (2), 127−136.
(24) Keremu, A.; Aimaiti, A.; Liang, Z.; Zou, X. Role of the HDAC6/STAT3 Pathway in Regulating PD-L1 Expression in Osteosarcoma Cell Lines. *Cancer Chemother. Pharmacol.* **2019**, *83* (2), 255−264.
(25) Skipper, P. L.; Tannenbaum, S. R.; Thilly, W. G.; Furth, E. E.; Bishop, W. W. Mutagenicity of Hydroxamic Acids and the Probable Involvement of Carbamoylation. *Cancer Res.* **1980**, *40* (12), 4704−4708.
(26) Shen, S.; Kozikowski, A. P. Why Hydroxamates May Not Be the Best Histone Deacetylase Inhibitors—What Some May Have Forgotten or Would Rather Forget? *ChemMedChem* **2016**, *11* (1), 15−21.

https://dx.doi.org/10.1021/acsmedchemlett.0c00395
ACS Med. Chem. Lett. XXXX, XXX, XXX−XXX